Chapter 5

Non-Toxic $CuInS_2$ Quantum Dots Sensitized Solar Cell with Functionalized Thermoplast Polyurethane Gel Electrolytes

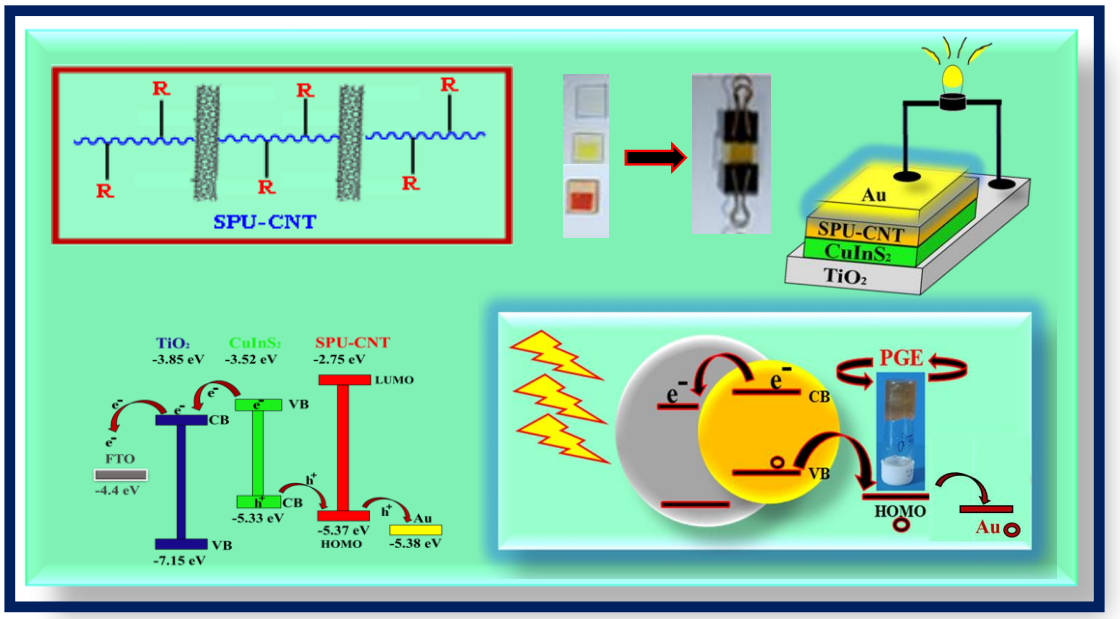

5.1 Introduction

A variety of photovoltaic solar cells was proposed and the photovoltaic technology can be classified in to three types; (1) First generation solar cells (2) Second generation solar cells (3) Third generation solar cells.[163,164] The first generation solar cell is based on mono or polycrystalline silicon, which is predominant technology on the market. This generation of solar cells is suffered from the high cost of manufacturing, installation and require a very purified silicon as a raw material. The second generation is based on the thin film technologies.[165,166] The most used materials in this case are amorphous silicon, cadmium telluride, copper indium gallium diselenide, copper indium diselenide and gallium arsenide. There are several disadvantages of this generation solar cells are: the amorphous silicon is easily degradable, cadmium is highly toxic, tellurium is a rare element and the other types of thin film have higher manufacturing costs, however, they have lower efficiency than first generation.[37,167] The new technologies should allow reduction of the manufacturing costs of devices. Quantum dots sensitized solar cells have drawn a lot of attention during past decade because of the possibility of boosting the energy conversion efficiency[16,168] beyond the traditional Shockley and Queisser limit of 32 % for silicon solar cells.[169,170] The QDs used in photovoltaic contains one or several toxic metals such as CdS, CdSe, CdTe, PbS, PbSe, SnS, and SnSe.[171,172] Due to high toxicity of the heavy metals that the QDs are made up of there is some concern about the toxicity of the QDs and their toxicology behaviors.[171] The International Agency for Cancer Research (IARC), classified the cadmium and lead metals are type-I carcinogen materials which can grow the tumors in lungs, prostate, injection site and other tissues.[171,172] An 8 h inhalation exposure of 5 Cd mg/m^3 for human is considered lethal and 1 mg Cd/m^3 is considered immediately dangerous for life. And the prolonged exposure to Cd can induce nephrotoxicity, osteotoxicity and immunotoxicity.[171] Recently, quantum dots sensitized solar cells are based on highly toxic Cadmium and lead

chalcogenides, hence due to their toxic behavior on health and environment the future commercialization is doubtful. In this sense, need a development of a green and environment friendly alternative materials i.e., Cadmium (Cd) and lead (Pb) free materials are introducing in the QDSSCs. Recently, the non-toxic ternary semiconductor chalcogenides were used in solar cells application with the general formula $A^{I}B^{III}X_2$. Ternary semiconductor $CuInS_2$ has a direct band gap of 1.5 eV, good radiation stability and a having high absorption coefficient 10^5 cm^{-1} which is considered as an ideal material for efficient solar cells. Copper indium sulfide ($CuInS_2$) is a non-toxic and an environment friendly chalcopyrite semiconductor and $CuInS_2$ is an ideal sensitizer because it has large absorption coefficient and tunable band gap. Theoretically, according to the Shockley-Queisser limit the expected power conversion efficiency of $CuInS_2$ based solar cell is reaches to 30-32 %. Carbon nanotubes are one-dimensional cylindrical structure have more attracted for photovoltaic applications because of their tunable band gap, optical and electronic properties.[173-175] The functionalization increases the hydrophilic nature of the CNTs resulting the aqueous solubility nature of the of the carbon nanotube increases. Various methods are reported for the CNTs-polymer nanocomposites such as solution casting, melt mixing, electrospinning, in situ polymerization and surface-assisted processing of CNTs-polymer composites.[176,177] The electrical conductivity of polymer matrix was increases with the attachments of the CNTs with polymer matrix.[178,179] The presence of the carbon nanotubes in polymer gel electrolytes which are facilitate the hole transport ability of the gel electrolytes.[180,181] The hole transport stability of the polymer gel electrolyte may increase the hole acceptance ability of the prepared polymer nanogel. Our assumption is to develop CNTs tagged polymer gel electrolytes as a better hole transporting agent using non-toxic quantum dots to fabricate photovoltaic device with better performance.

In the present work, the functionalized MWCNTs was chemically tagged with the main chain of the thermoplastic polyurethane polymer matrix through in *situ*-polymerization process, and which is further functionalized to developed the novel polymer nanogel electrolytes i.e., hole transport materials for the QDSSCs. The Ni metal used as a counter electrode and optimized the annealing temperature for the suitable matching of work function Ni with HOMO energy levels of the prepared functionalized polymer nanogel to obtained better the photovoltaic performance. The prepared functionalized polymer nanogel ware used to the fabricated the QDSSCs with $TiO_2/CuInS_2$ photoanode.

5.2 Results and Discussion

5.2.1 Synthesis of MWCNTs-Tagged Polyurethane and its Functionalized Ionomer

The schematic reaction for the functionalization of the MWCNT and the chemically f-MWCNT-tagged polyurethane polymer (PU-CNT) proceed through polymerization reaction and its subsequent functionalization (SPU-CNT) are shown in **Scheme 5.1**. ^{1}H NMR and FTIR spectroscopic measurements were used to confirm the functionalization of MWCNTs, chemical tagging of the f-MWCNT with main polymer chain and its subsequent functionalization of polyurethane polymer. ^{13}C NMR patterns of the pristine MWCNTs and functionalized MWCNT (f-MWCNT) are shown in **Figure 5.1a.** The functionalized MWCNT shows two new intense peaks at chemical shift δ = 207 ppm and 31 ppm for the carboxylic -COOH and alcoholic (-ROH) protons, respectively, while these peaks are absent in pristine CNT, which confirm the functionalization of the multiwalled carbon nanotubes. **Figure 5.1b** represents the FTIR measurements of the pristine and functionalized MWCNTs. In the FTIR measurements,

functionalized CNTs shows the peaks at 3221 and 2965 cm^{-1} for -OH asymmetric and symmetric stretching frequency, respectively, which indicate the presence the -OH group in carbon nanotubes,

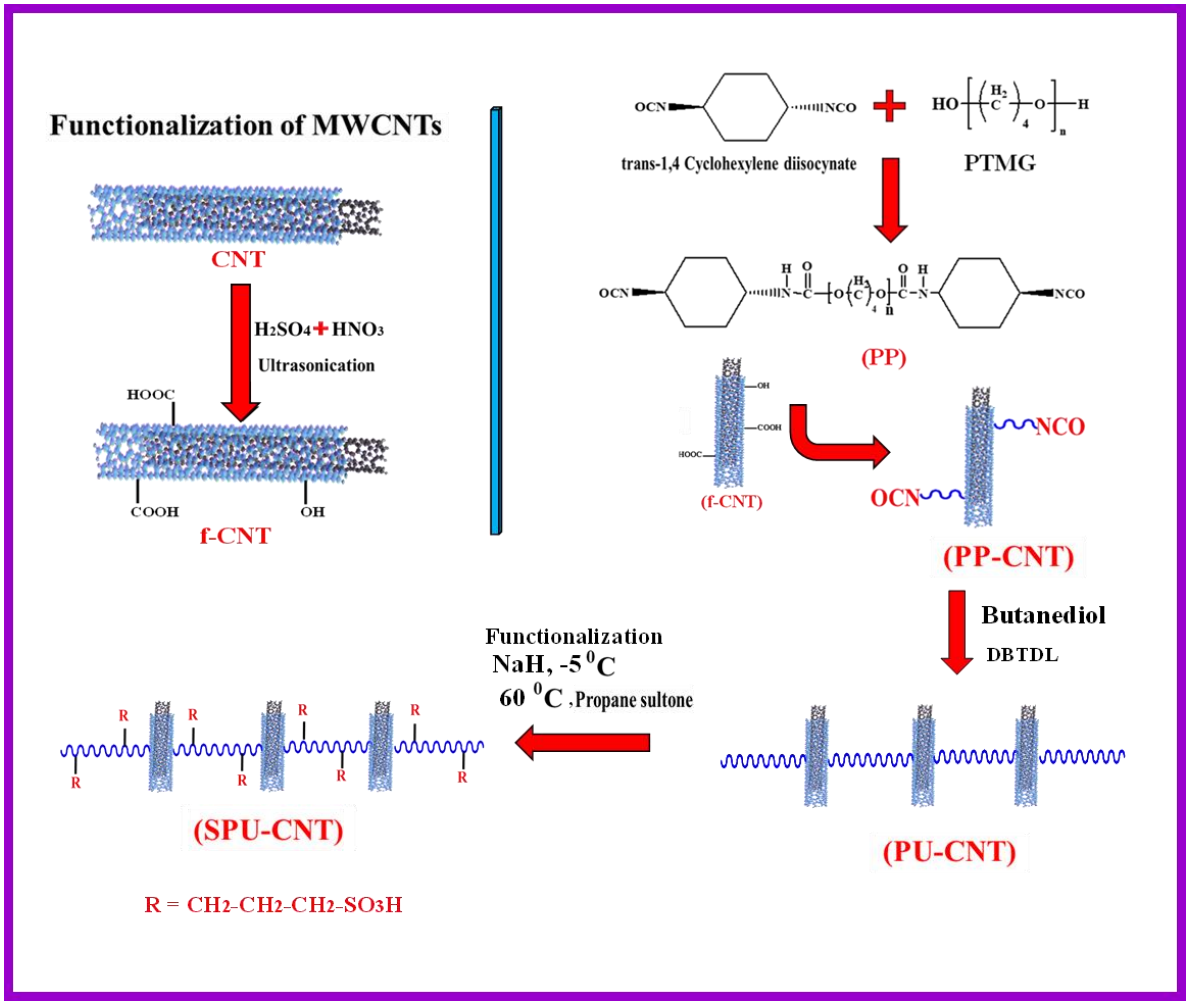

Scheme 5.1: functionalization of MWCNTs and synthesis of f-MWCNT tagged polyurethane polymer (PU-CNT) and its subsequent functionalized polymer (SPU-CNT).

and C-O bands characteristics of carbonyl functional group on MWCNT-COOH surface was observed at 1760, 1637, and 1563 cm^{-1}. The peak at 1563 cm^{-1} is related to the carboxylate anion stretching mode which is the clear indication of -COOH group present on the surface of the CNTs,

and these bands are not present in pristine MWCNT, which also indicate the presence of –OH and –COOH group on the surfaces of the MWCNT after functionalization. The UV-visible spectroscopy measurement of pristine and functionalized MWCNT are shown in **Figure 5.1c**. The pristine CNT shows a peak at 225 nm is due to $\pi \rightarrow \pi^*$ transition and after the functionalization of CNT, the $\pi \rightarrow \pi^*$ is blue shifted peak at 220 nm is observed and another new peak is also appearing at 298 nm is due to $n \rightarrow \pi^*$ transition which is the clear indication of the functionalization of CNT. The pristine CNTs shows a peak at 225 nm is due to $\pi \rightarrow \pi^*$ transition and after the functionalization of CNTs, the $\pi \rightarrow \pi^*$ is blue shifted peak at 220 nm was observed and another new peak was also appearing at 298 nm is due to $n \rightarrow \pi^*$ transition which was the clear indication of the functionalization of CNTs. The **Figure 5.2a** represents the ^{1}H NMR spectra of pure polyurethane (PU), f-MWCNT-tagged polyurethane (PU-CNT) and sulfonated polyurethane polymer (SPU-CNT). The pure PU shows a characteristics peak at chemical shift $\delta = 7.94$ ppm for >NH proton and after the tagging of f-CNT with polymer chains, there are two new peaks observed at chemical shift values of $\delta = 4.47$ and 1.03 ppm for the indication of alcoholic proton on the surfaces of carbon nanotube which confirm the successful functionalization of CNTs with the polymer chains, and its subsequent functionalized polymer shows a new intense peaks at chemical shift values $\delta = 8.45$ ppm for the -SO_3H proton, and another two new peaks at $\delta = 2.07$ ppm, and 1.6 ppm for -CH_2 protons of the propane sultone group, and these all peaks are absence in PU-f-CNT and PU, hence, confirm the clear sign of the attachments of the sulfonate group on the main polymer chains of PU-CNT. The FTIR measurements of prepolymer (PP), CNTs-tagged prepolymer (PP-CNT), CNT-tagged polyurethane (PU-CNT) and sulfonated polyurethane polymer (SPU-CNT) are shown in **Figure 5.2b**. In the FTIR measurements, the prepolymer shows a characteristics peak at 3305 cm^{-1} due to hydrogen bonded >NH group (stretching frequency)

present in prepolymer in hard segments and this peak is shifted to 3325 cm^{-1} in the CNTs-tagged prepolymer and it becomes broads in sulfonated polyurethane polymer and appears at 3389 cm^{-1}, and the peak appears at 1760 cm^{-1} is due to the presence of -NCO group in both prepolymer (PP) and CNTs- tagged pre-polymer (PP-CNT), while this peak disappears in CNTs-tagged polyurethane polymer (PU-CNT) which indicate that the chain extension of polymer after the reaction with butanediol. The subsequent functionalized polymer shows a new peak at 1183 cm^{-1} is due to symmetrical stretching vibration of the -S=O linkages after the sulfonation of the polymer and this peak is not observed in PU-CNT, which indicates the successful functionalization of the polymer. The UV-visible spectroscopic measurements are used to analyse the interaction between the CNTs and polymer chains.

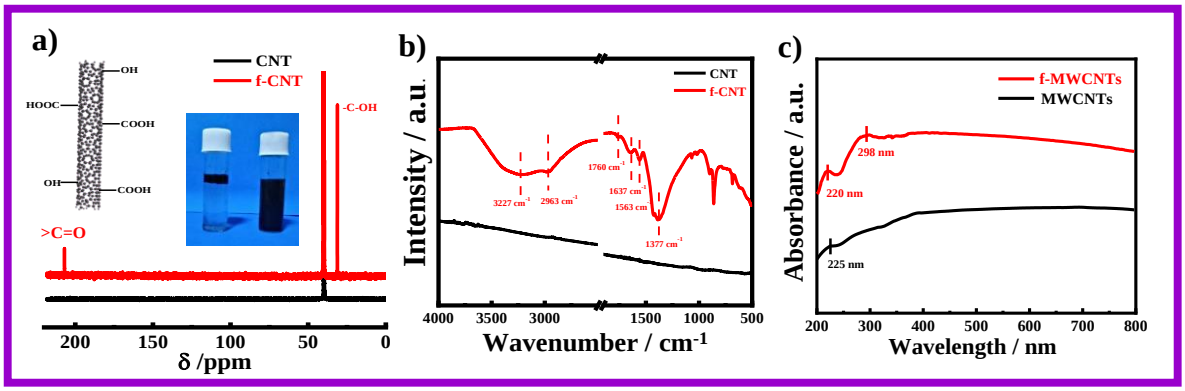

Figure 5.1: (a) ^{13}C NMR spectroscopy measurements for pristine and functionalized MWCNTs, (b) FTIR measurements of pristine and functionalized MWCNTs, (c) UV-vis absorption measurements of pristine and functionalized MWCNTs,

Figure 5.2c represents the UV-visible spectroscopic measurements of the PP, PP-CNT, PU-CNT and SPU-CNT. The peak appears at 268 nm in PP is due to n → π^* transition and it is red shifted to 269 nm and another new peak appears at 355 nm due to the presence of f-MWCNT in PP-CNT and further these peaks have shifted to 271 and 363 nm in PU-CNT after the chain extension through butanediol. The functionalized polymer shows two peaks at 271 nm, due to n → π^* transition of urethane linkage and another one at 369 nm assigned as n → π^* transition due to the presence of polar sulfonate group in polymer chains. Raman spectroscopic measurements are very important technique for the analysis of CNTs, as it gives the information about degree of structural disorder. Raman spectroscopy measurements is very important technique for the analysis of CNTs, because it gives the information about degree of structural disorder.

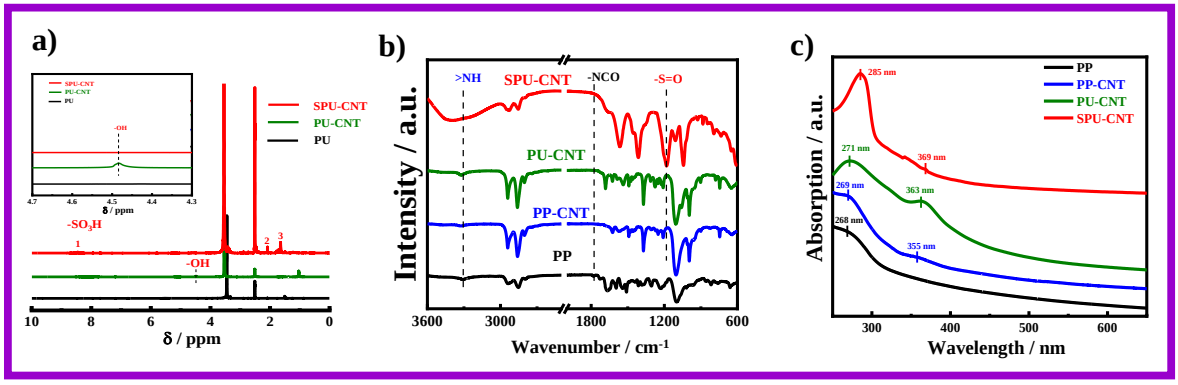

Figure 5.2: (a) ^{1}HNMR spectra of PU, PU-CNT and SPU-CNT polymer, (b) FTIR spectroscopic pattern for PP, PP-CNT, PU-CNT, and SPU-CNT polymer, (c) absorption spectroscopic measurements of PP, PP-CNT, PU-CNT, and SPU-CNT polymer.

The Raman spectra of pristine-CNT, functionalized-CNT, PP, PP-CNT and PU-CNT are shown in **Figure 5.3a.** It is observed that the spectra of pristine and functionalized CNTs are quite similar and have same pattern, which indicate that the structure of the graphene sheet does not suffer from major damages during the functionalization. Interestingly, this is a good sign as critical condition of oxidation may cause higher damage to the structure of MWCNTs. It is expected that the oxidation of MWCNTs creates desired functional group along with the usual structure of MWCNT. The Raman G band (G = graphite) of CNTs is important which is related to the graphite structure (carbon atoms high-frequency E_{2g} first order mode) and stems from the tangential shearing mode, D band arises due to structural defect and G′ band is an overtone of D band. The G band appears at 1569 cm^{-1} for pristine CNTs and it has shifted to higher wavenumber at 1575 cm^{-1} in functionalized CNT and the similar trend is obtained for D and G′ band. The integrated intensity ratio of the D and G bands can be used to calculate the density of the defects in CNTs structure and the higher the value of the I_D/I_G ratio, higher will be the defect density.[182,183] In pristine MWCNTs, I_D/I_G ratio value to be 0.961 is obtained which is similar to the literature value[184] while in the functionalized MWCNTs the I_D/I_G ratio value shifted to 0.985, which indicate that the more defect was arises after the functionalization. The low intense G' band was appearing in both PP-CNT and PU-CNT while absent in PP, which indicate that, the successful attachment of CNT with main polymeric chains. The thermogravimetric measurement technique ware used to estimate the thermal stabilities of the PP, PP-CNT, PU-CNT and SPU-CNT. The **Figure 5.3b** represents the thermal behavior of the prepolymer, polymer and functionalized polymer. The presence of the hard and soft segments in the polymeric chain of the both pure and functionalized polymer shows the two stages degradation and the functionalized polymer have lower degradation temperature as compared to pure polymer. The weight loss at lower temperature

is due to the degradation of the hard segment of the polymer chain and the soft segments is degraded at relatively higher temperature. In the SPU-CNT polymer, the initial weight loss is observed due to its sulfonate group. The degradation temperatures are found to be 273^0, 361^0, 367^0 and 171 ^{0}C for PP, PP-CNT, PU-CNT and SPU-CNT, respectively. The presence of MWCNT enhances the thermal stability while due to sulfonation quite lower thermal stability is observed in SPU-CNT. This is to mention that the degradation temperature is measured at the temperature corresponds to 5 % weight loss. The functionalized polymer (SPU-CNT) is thermally stable up to 170 ^{0}C hence, it is suitable for the solar cell technology. The melting behavior of the synthesized polymer is measured through differential scanning calorimetric measurements and are shown in **Figure 5.3c.** The melting temperature of the prepolymer is 37.9 ^{0}C and after tagging of CNTs with prepolymer increases its crystalline nature, due to which, the melting temperature of the prepolymer increases to 38.32 ^{0}C.

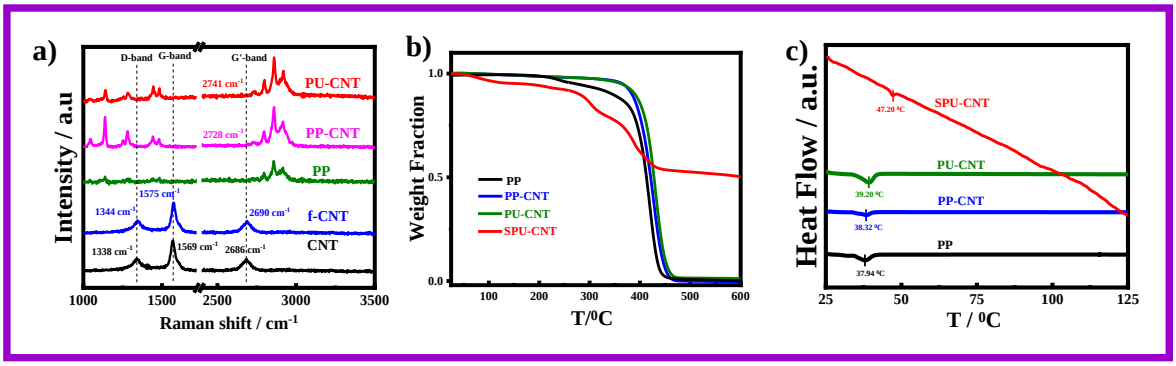

Figure 5.3: (a) Raman spectroscopic pattern for MWCNTs, f-MWCNTs, PP, PP-CNT, PU-CNT, and SPU-CNT polymer, (b) Thermogravimetric measurements for PP, PP-CNT, PU-CNT, and SPU-CNT polymer, (c) Differential scanning calorimetry measurements for PP, PP-CNT, PU-CNT, and SPU-CNT polymers.

Further, the melting temperature increases to 39.2 ^{0}C for chain extended polymer by using the butanediol, and due to presence of sulfonate group in SPU-CNT, the interaction between ionic – SO_3H and polar >NH group of the hard segments is higher, resulting the functionalized polymer (SPU-CNT) having the higher melting temperature at 47.2 ^{0}C. The heat of fusion values are determined to be 22. 2, 24.5, 28.4 and 11.6 J g^{-1} for PP, PP-CNT, PU-CNT, and SPU-CNT, respectively. The presence of the MWCNTs in the polymeric chain increases the melting temperature as well as heat of fusion while in the sulfonated polymer heat of fusion decreases due to presence of sulfonate group which may reduce the crystallinity of the functionalized polymer.

5.2.2 Electrochemical Behavior of CNTs tagged Polyurethane and its Ionomer

Electrical conductivity of the prepared electrolytes directly affects the photovoltaic performance of the fabricated devices hence, the prepared polymer electrolytes having good ionic conductivity

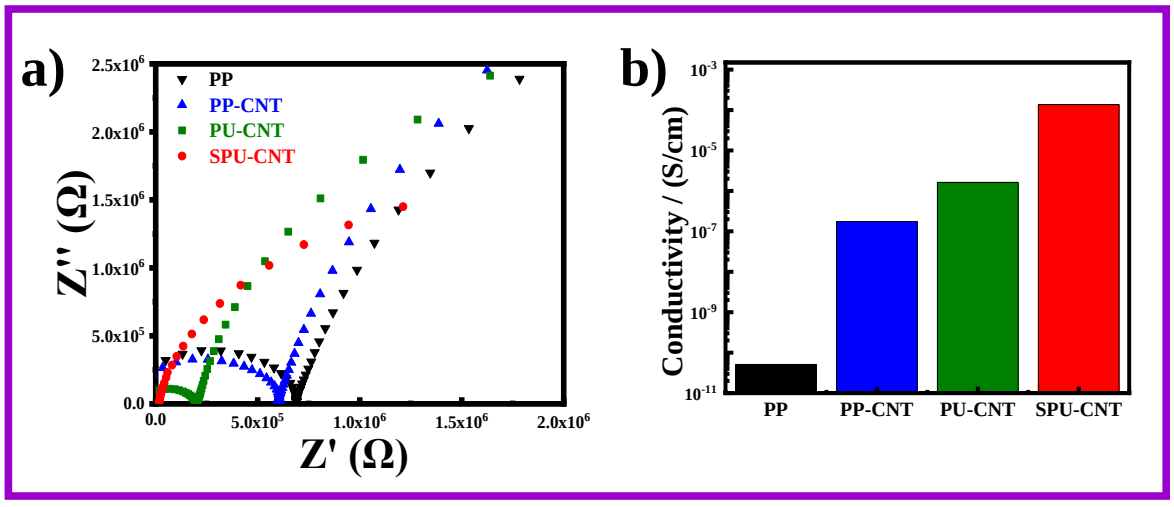

Figure 5.4: (a) Nyquist plots for the indicated pure and functionalized PUs, (b) ionic conductivity for PP, PP-CNT, PU-CNT, and SPU-CNT polymers.

is responsible for the better hole transformation in fabricated device in operational mode. The ionic conductivity of the synthesized polymer is estimated through the electrochemical impedance spectroscopy measurement, and the Nyquist plots are used to calculate the polarization resistance of the polymer using the fit and simulation method (**Figure 5.4a**). The resistance of PP is found to be $3.594 \times 10^8\ \Omega$ and with the attachment of MWCNTs with polymer chain it decreases to $1.74 \times 10^5\ \Omega$ for PP-CNT due to presence of π-framework which provide the charge transport medium for better charge transportation. Further, reduction of resistance for chain extended polymer (PU-CNT) is observed at $1.133 \times 10^8\ \Omega$ as compared to PP. **Figure 5.4b** represents the ionic conductivity of the PP, PP-CNT, PU-CNT, and SPU-CNT. The attachment of ionic sulfonate moiety in the main polymeric chain in SPU-CNT exhibit the resistance of $1.339 \times 10^2\ \Omega$. **Table 5.1** represents the corresponding ionic conductivity and the functionalized polymer exhibits the ionic conductivity which belongs to semiconducting range (1.367×10^{-4} S cm^{-1}); hence, it is suitable for the solar cell's applications. However, it is observed that the ionic conductivity increases after tagging of MWCNT with the polymer chains which has further enhanced through functionalization.

Table 5.1: The resistance and conductivities of pure, CNT-tagged and functionalized polymer.

S.N	Sample	Resistance (Ω)	Conductivity (S cm^{-1})
1.	**PP**	$\mathbf{3.594 \times 10^8}$	$\mathbf{5.094 \times 10^{-11}}$
2.	**PP-CNT**	$\mathbf{1.052 \times 10^5}$	$\mathbf{1.740 \times 10^{-7}}$
3.	**PU-CNT**	$\mathbf{1.133 \times 10^4}$	$\mathbf{1.616 \times 10^{-6}}$
4.	**SPU-CNT**	$\mathbf{1.339 \times 10^2}$	$\mathbf{1.367 \times 10^{-4}}$

Cell durability is a key parameter for the development and fabrication of the photovoltaic devices which is directly influenced by the developed materials used in device fabrication. The low life cycle of the fabricated devices depends upon the corrosiveness of the developed active materials. The potentiodynamic polarization measurement with three electrode setups assembled in a glass cell was used to calculate the corrosive nature. Ag/AgCl was used as a reference electrode, mild steel was used a working electrode and platinum as a counter electrode. The dimension of the working electrode was 3 × 1 × 01 cm^3 with an active area 1 cm^2 and was dipped in 0.5 M H_2SO_4 acid solution for corrosion testing.

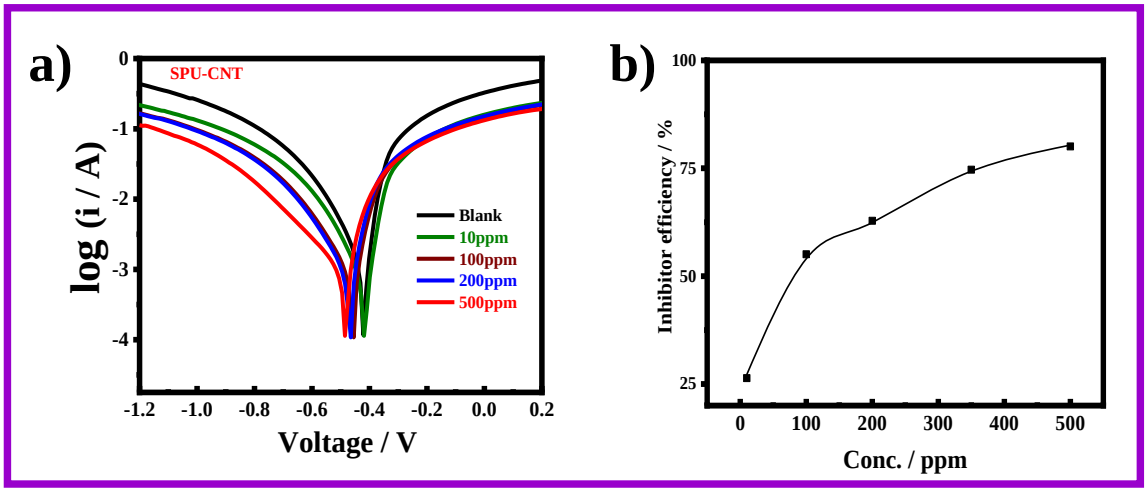

Figure 5.5: (a) potentidynamic polarization measurements of mild steel with and without the indicated inhibitors in 0.5 M H_2SO_4 solution; and (b) percentage inhibitor efficiency as a function of inhibitor (SPU-CNT) concentration.

The corrosion current densities and corrosion potential were determined by extrapolating cathodic and anodic current-potential characteristics of the linear polarization Tafel plots up to their intersection point. The inhibitor efficiency is calculated from the measured I_{corr} values using the following equation;

$$IE\ (\%) = \frac{I^0_{corr} - I_{corr}}{I^0_{corr}} \quad \text{.....5.1}$$

where, I_{corr} and I^0_{corr} are the current densities with and without the presence of inhibitors, respectively. **Figure 5.5a** represents the linear potentiodynamic polarization Tafel plots. The blank coupon (without inhibitors) was run to measure the I^0_{corr} and E^0_{corr} values and are found to be 2.96×10^{-6} A cm^{-2} and -0.419 volt, respectively. The corrosion current density decreases from 2.96×10^{-6} A cm^{-2} to 2.18×10^{-6} A cm^{-2} and corrosion potential has shifted from -0.419 to -0.422 V with the addition of 10 ppm concentration of the SPU-CNT with the inhibitors efficiency (η) of 26.25 %. **Table 5.2** represent the variations of the I^0_{corr}, E^0_{corr} and inhibitor efficiency (η) with increasing the inhibitors concentration. The 80.6% inhibitors efficiency is observed by using the 500 ppm concentration of the SPU-CNT polymer **(Figure 5.5b**). However, the anti-corrosiveness of SPU-CNT system is developed with higher inhibitor efficiency (η). Hence, the developed SPU-CNT system is suitable for the fabrication of the solar cell gel electrolyte.

Table 5.2: Corrosion current density, potential, corrosion rate density and percentage inhibition efficiency of functionalized polymer (SPU-CNT) at different concentration

Inhibitor	Inhibitor concentration (ppm)	Corrosion potential (v)	Corrosion rate density (µA / cm^2)	Inhibitor efficiency (%)
Blank	**-----**	**0.419**	**2.96**	**----**
SPU-CNT	**10**	**0.422**	**2.18**	**26.35**
SPU-CNT	**100**	**0.455**	**1.33**	**55.06**
SPU-CNT	**200**	**0.465**	**1.10**	**62.83**
SPU-CNT	**350**	**0.474**	**0.75**	**74.66**
SPU-CNT	**500**	**0.485**	**0.59**	**80.06**

5.3 Microscopic Characterization of $CuInS_2$ QDs

Transmission electron microscopic bright field image measurements was used to calculate the particle size and its distribution. The representative TEM bright field images are shown in **Figure 5.6a**. The average particle size of the synthesized $CuInS_2$ QDs is measured to be 2.5 nm and the size distribution histogram is shown in inset of **Figure 5.6a**. Santra et.al.[146] synthesized the $CuInS_2$ QDs and fabricated the QDSSCs with $TiO_2/CuInS_2$ photoanode using the polysulfide electrolytes with particle size 2.6 nm in range, hence, the synthesized QDs size are similar with literature and it is beneficial for the device fabrication. **Figure 5.6b** represent the FTIR spectroscopic measurements of prepared DDT capped $CuInS_2$ QDs. In FTIR spectra, the DDT capped $CuInS_2$ QDs appears a three bands around 2900 cm^{-1} i, e., at 2955, 2919 and 2850 cm^{-1} are assigned to $-CH_3$ asymmetric stretching, $-CH_2$ asymmetric and $-CH_2$ symmetric stretching vibration, respectively.[185] The bands appears at 720 cm^{-1} and 1259 cm^{-1} are corresponding to C–S stretching vibration and $-CH_2$-S wagging vibration. Hence, it can be affirmed that the surface

ligand is DDT and DDT-capped $CuInS_2$ QDs was formed. The UV-vis spectroscopic measurements of the prepared CuInS2 QDs are shown in **Figure 5.6c.** The characteristics absorption peaks for $CuInS_2$ QDs is 574 nm which ware consistent with literature report.[186,187]

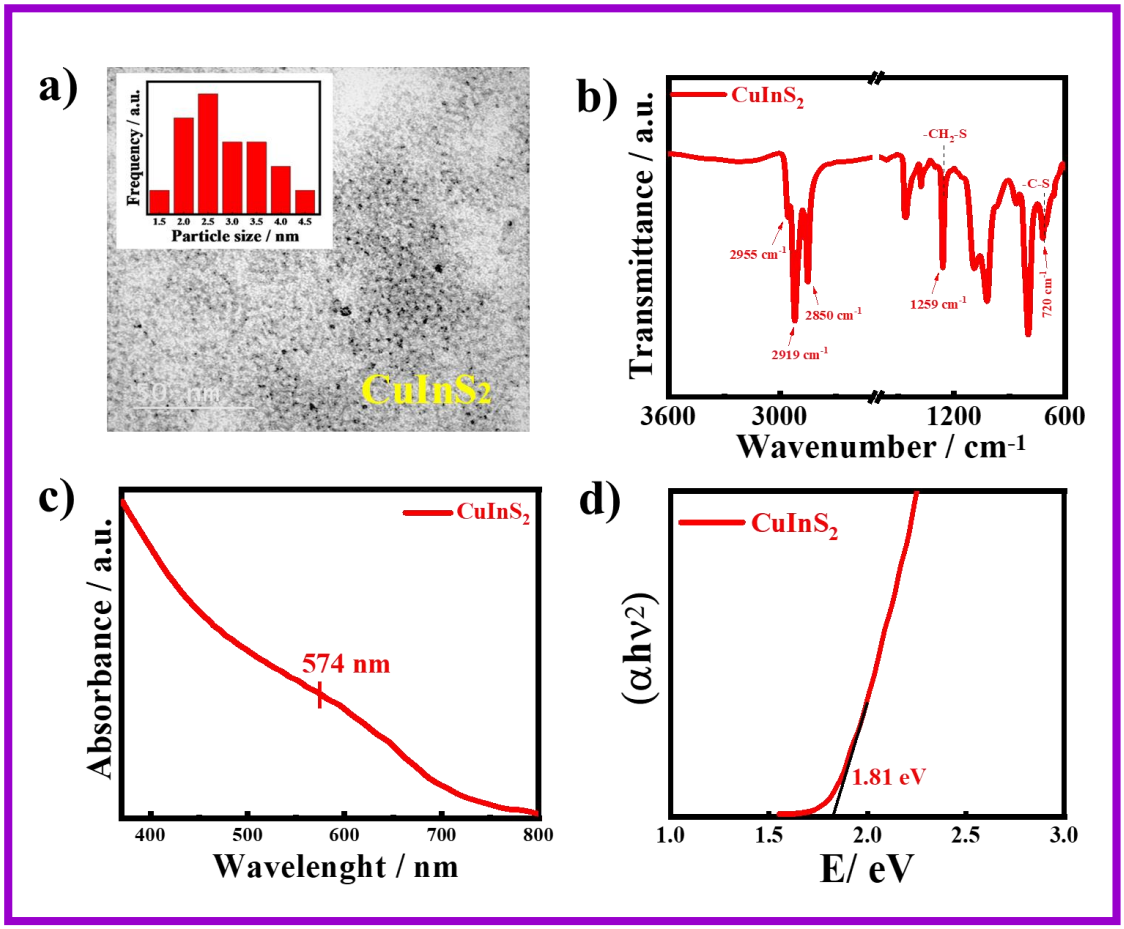

Figure 5.6: (a) TEM bright field image and particle size distribution, (b) FTIR spectra of the synthesized $CuInS_2$ QDs, (c) UV-vis absorption spectra of $CuInS_2$ QDs; (d) optical band measurement of $CuInS_2$ QDs.

The absorption band appears at 512 nm for pure $CuInS_2$ QDS (without any capping agents are used), a capping agents play a crucial role in absorption spectroscopy of the $CuInS_2$ QDs because it enhanced the absorption capability in visible region. The optical band gap is found to be 1.81 eV for $CuInS_2$ QDs, using the Tauc's plots and which are shown in **Figure 5.6d.**

5.4 Optical, and Electrochemical Properties of Polymer and QDs

The cyclic voltametric measurements are an important tool to analyzed the electrochemical behavior of the materials at electrode-electrolyte interfaces and to estimate the generated current with applying the voltage at specific scan rate. During the redox reaction, a polymer chains converted in to negatively charge species in reduction reaction, whereas in oxidation reaction it changed in to positively charged species. There are two different types of the peaks are obtained in CV measurements, one for the reduction process and produced the negative current and other for the oxidation process and generates the positive current. The HOMO and LUMO energy levels of the materials are calculated from the onset of the oxidation and reduction potential of the CV measurements, respectively. The rate of transportation of electrons and holes are depending upon the HOMO and LUMO energy levels of the materials. **Figure 5.7a** represent the current-voltage curve for MWCNTs-tagged PUs and functionalized PUs polymer (SPU-CNT) form the CV measurements.

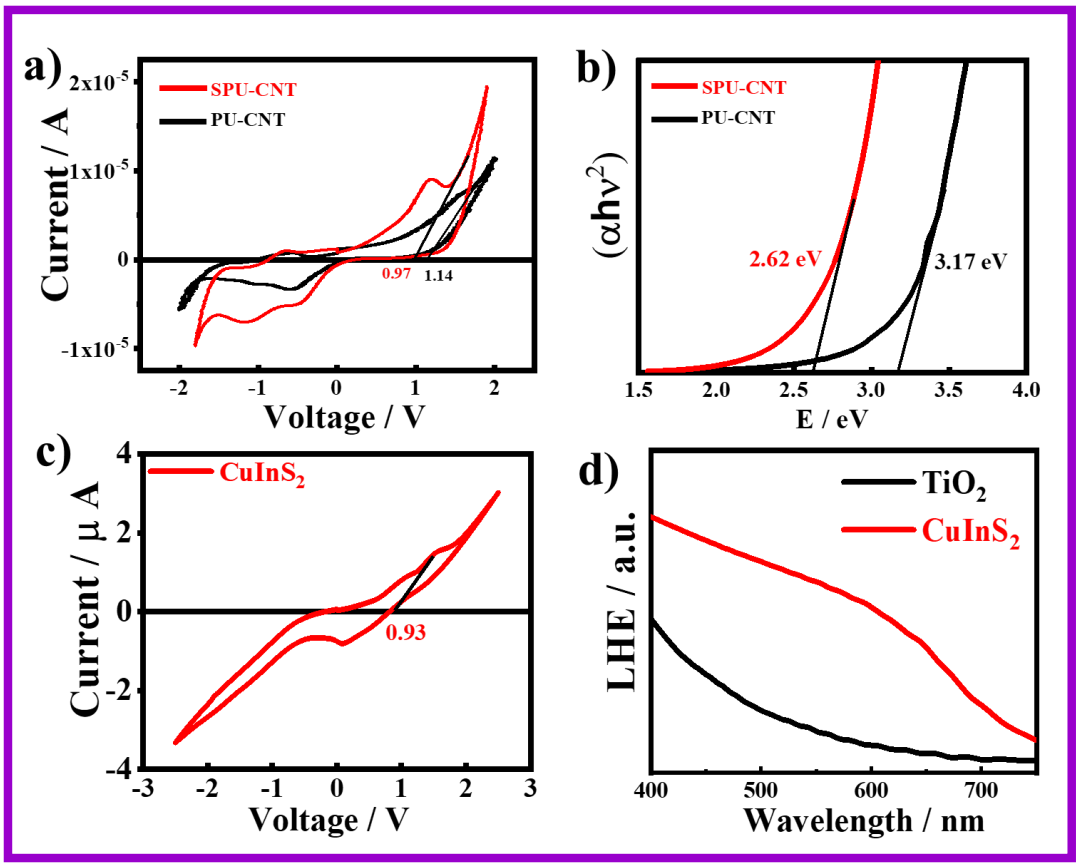

Figure 5.7: (a) CV measurements of PU-CNT and SPU-CNT polymers, (b) optical band gap measurements of PU-CNT and SPU-CNT polymers, (c) CV measurements of $CuInS_2$ QDs, (d) relative light harvesting efficiency of FTO/TiO_2 and FTO/TiO_2/$CuInS_2$ QDs.

The E_{OX} values are 1.14 and 0.97 for functionalized and pure CNT-tagged polyurethane polymer, respectively, and E_{HOMO} values are measured to be -5.54 eV and -5.37 through equation 1. The optical band gap of the PU-CNT and SPU-CNT are calculated by using the Tauc's plots and the values are 3.17 eV and 2.62 eV for PU-CNT and SPU-CNT, respectively which are shown in **Figure 5.7b** and it was observed that the optical band gap are decreases with the functionalization,

similar with literature. The E_{LUMO} value is calculated by using the optical band gap value in equation 2 and the E_{HUMO} value is estimated through CV measurement, and the calculated values of E_{LUMO} are -2.37 and -2.75 eV for the PU-CNT and SPU-CNT, respectively. **Figure 5.7c** represent the CV measurements of the $CuInS_2$ QDs, and the E_{OX} value of $CuInS_2$ QDs is calculated as 0.93 V and E_{HOMO} and E_{LUMO} values are -5.33 eV and -3.52 eV respectively as calculated using the equation (1) and (2). For developing the efficient photovoltaic devices, the active materials have more light harvesting efficiency and higher the value of LHE, higher will be the generation of excitons under the exposure of the solar radiation. The light harvesting efficiency (LHE) of TiO_2 and $TiO_2/CuInS_2$ is shown in **Figure 5.7d,** the LHE value of $CuInS_2$ QDs is higher as compared to TiO_2 and it becomes red shifted hence the use of $CuInS_2$ QDs as an active material is beneficial for device fabrication.

5.5 Energy-Profile Diagram, Hole Transportation and Device Structure

On combining E_{HOMO}, E_{LUMO} of polymers and the VB and CB of the prepared QDs with various counter electrode to draw the energy profile diagram shown in **Figure 5.8 (a-c),** and find the suitable matches for better hole transportation. **Figure 5.8a** represent the energy profile diagram for the prepared SPU-CNT polymer gel electrolyte, synthesized $CuInS_2$ QDs and platinum metals used as a counter electrode. The solar light exposed on the photoanode of the fabricated QDSSCs, the $CuInS_2$ absorbs the solar light and generates the exciton (electrons hole-pair) and the excited electron transfer from the conduction band (CB) of $CuInS_2$ to CB of TiO_2 and hole are transported from Valence band (VB) QDs to counter electrode through gel electrolyte. The rate of transportation of hole is slow due to larger energy difference between HOMO energy levels of gel electrolytes

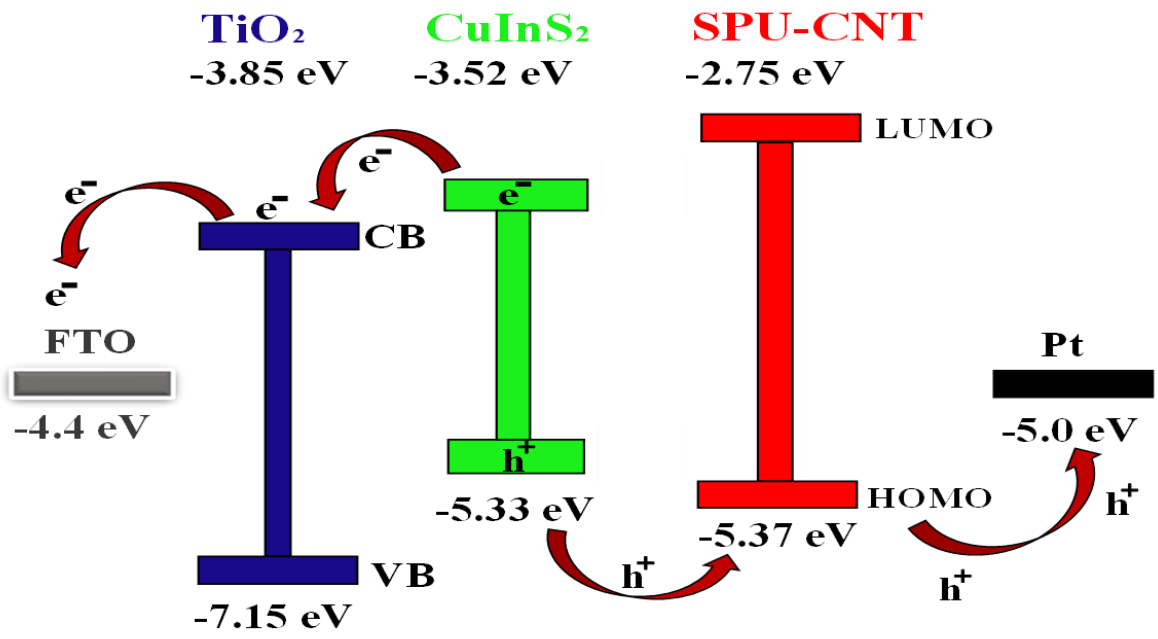

Figure 5.8: (a) Energy profile diagram of TiO_2, $CuInS_2$ with SPU-CNTs gel electrolyte using the platinum as counter electrode.

Figure 5.8b represent the energy profile diagram for the prepared SPU-CNT polymer gel electrolyte, synthesized $CuInS_2$ QDs and nickel (Ni) metals used as a counter electrode. The rate of transportation of hole is slightly higher as compared to the platinum electrode, due to smaller energy difference between HOMO energy levels of gel electrolytes and energy level of nickel counter electrode.

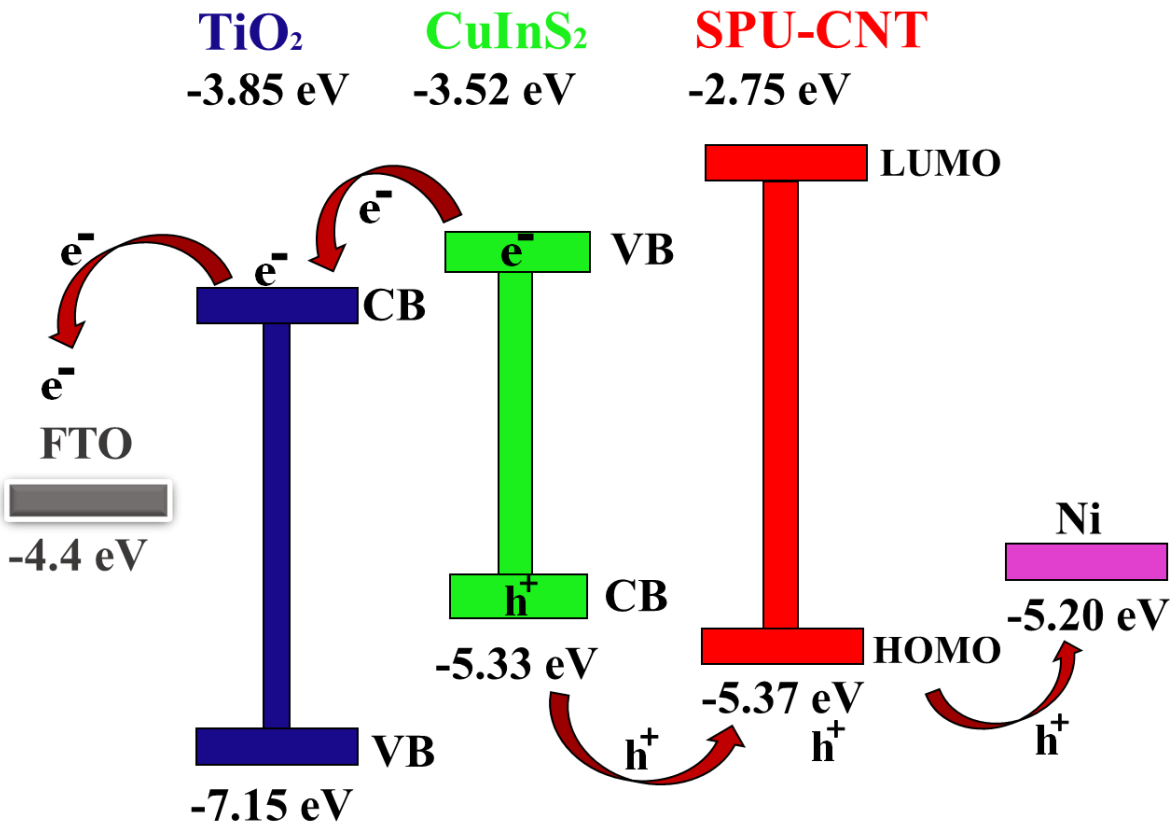

Figure 5.8: (b) Energy profile diagram of TiO_2, $CuInS_2$ with SPU-CNTs gel electrolyte using the nickel as counter electrode.

Figure 5.8c describes the energy profile diagram for the prepared SPU-CNT polymer gel electrolyte, synthesized $CuInS_2$ QDs and gold (Au) metals used as a counter electrode. The rate of transportation of hole is fast due to very less energy difference between HOMO energy levels of gel electrolytes and energy level of Au (gold) counter electrode. Hence, it was observed that the hole transportation is fast in this case and the fabricated devices performance is better as compared the platinum and nickel counter electrode.

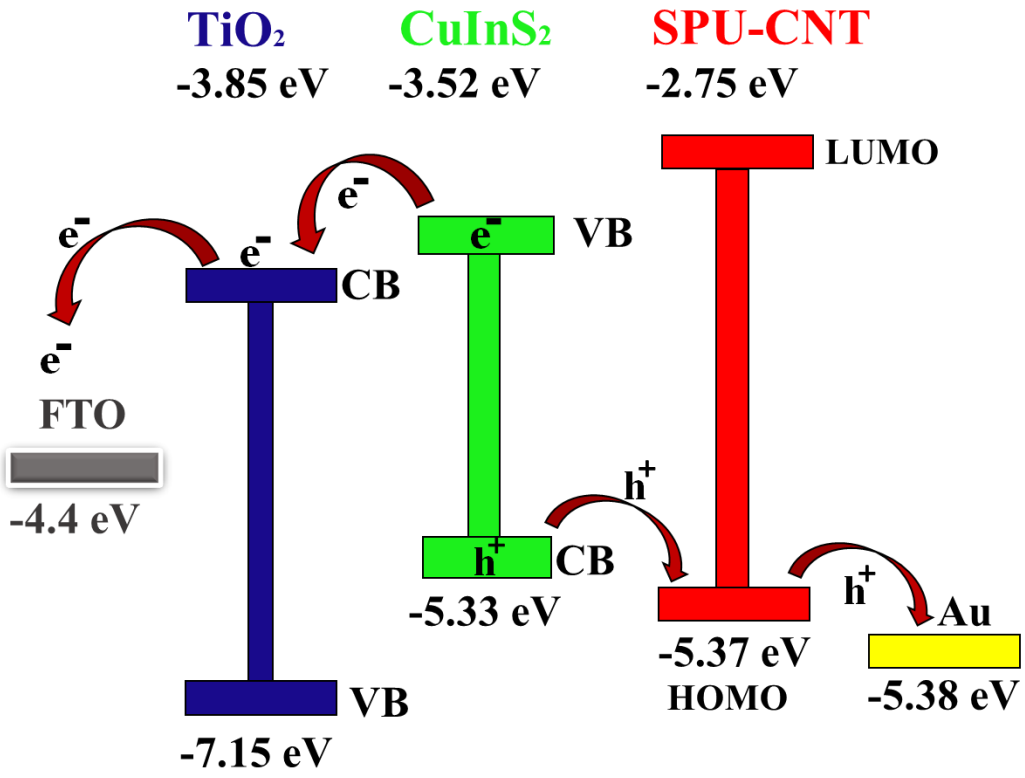

Figure 5.8: (c) Energy profile diagram of TiO_2, $CuInS_2$ with SPU-CNTs gel electrolyte using the gold (Au) as counter electrode.

The energy profile diagram of the prepared polymers (SPU-CNT), $CuInS_2$ QDs with Au (gold) counter electrode is shown in **Figure 5.9a**. From the energy profile diagram, it was concluded that the rate of hole transportation is fast from VB of the QDs to the HOMO energy levels of the polymer gel electrolytes because the energy levels VB of QDs and HOMO of gel electrolyte is very close (difference between these is very low i.e., 0.04), while the energy difference between

HOMO levels of gel electrolyte and energy levels of the platinum counter electrode is quit high and its value is 0.37, so the hole transportation is slow resulting the devices performance is low.

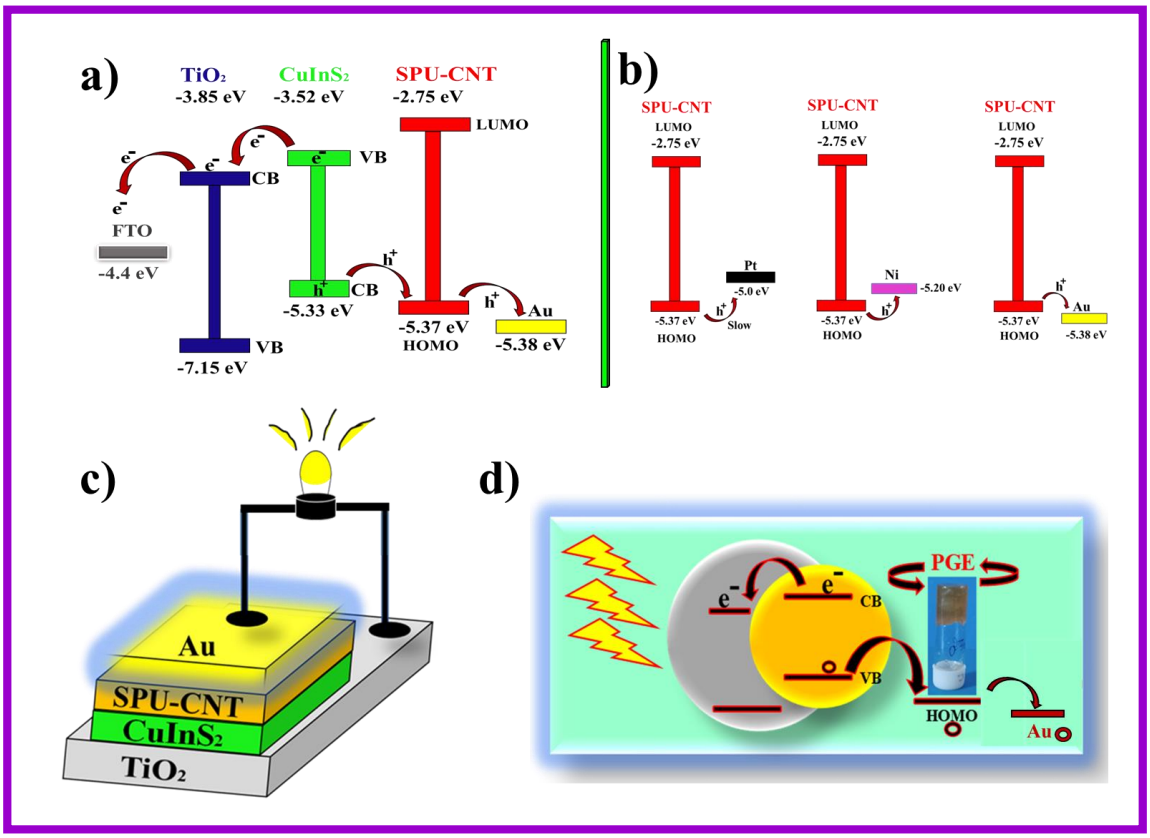

Figure 5.9: (a) Energy profile diagram of TiO_2, $CuInS_2$ with SPU-CNTs gel electrolyte using the gold as counter electrode; (b) comparative energy levels of the SPU-CNTs with various counter electrode (Pt, Ni, and Au) showing the transportation of holes, (c) schematic layer structure of fabricated QDSSCs, (d) schematic representation of solar excitation mechanism and hole transportation behavior inside the fabricated QDSSCs.

However, another counter electrode is essential for the better performance of the device and which energy level is close to HOMO energy level of the developed polymer (SPU-CNT) gel electrolytes for the better hole transportation and device performance. Hence, thin film of Nickel metal was used as a counter electrode further it was annealed at 100 ^{0}C for the 30 min and cooled at room temperature and the prepared Nickel counter electrode work function is -5.20 eV which are closer to the HOMO energy levels of the gel electrolytes and difference between these energy levels is 0.17 and the comparative band energy diagrams of prepared SPU-CNT polymer, $CuInS_2$ QDs with Pt, Ni and Au (gold) counter electrodes are shown in **Figure 5.9b**. Which may give the information about hole transport ability between the gel electrolytes and counter electrodes, the hole transportation is better in Au (gold) counter electrode than both platinum and nickel counter electrode due to less energy difference, hence device performance may better in Au counter electrode. The **Figure 5.9c** represents the schematic diagram of the layer by layer structure of the TiO_2/$CuInS_2$ photoanode designed along with a polymer gel electrolyte was fabricated QDSSCs and the schematic reaction taking place in the fabricated devices are shown in **Figure 5.9d,** when the solar irradiation was fall on the prepared photoanode the $CuInS_2$ QDs absorbs the light and generates the exciton (electron-hole pairs) and the excited electron transfer from the CB of $CuInS_2$ to the CB of the TiO_2 levels and further transfer to the external circuit and the hole are transported from the VB of $CuInS_2$ QDs to the HOMO energy levels, followed by transfer to the counter electrode to complete the circuit and resulting flow the electricity.

5.6 Photovoltaic Performance

The photocurrent-voltage (J-V) characteristics curves of the TiO_2/$CuInS_2$ photoanode with prepared SPU-CNT polymer gel electrolytes by using the various counter electrode (Pt, Ni and

Au), to fabricates the QDSSCs under 1 sun solar radiation with light intensity of 100 mW cm^{-2} are shown in **Figure 6a**. The $TiO_2/CuInS_2$ photoanode using the prepared polymer electrolyte with platinum electrode show the high fill factor value of 0.56 and 0.71 V open circuit voltage (V_{oc}) while the photocurrent density is low J_{max} ~1.55 mA cm^{-2} resulting low power conversion efficiency (η) = 0.62 % observed. Therefore, an improvement is needed in terms of power conversion efficiency. The power-voltage curve is shown in **Figure 6b,** which describes the variation of the maximum power output under solar radiation.

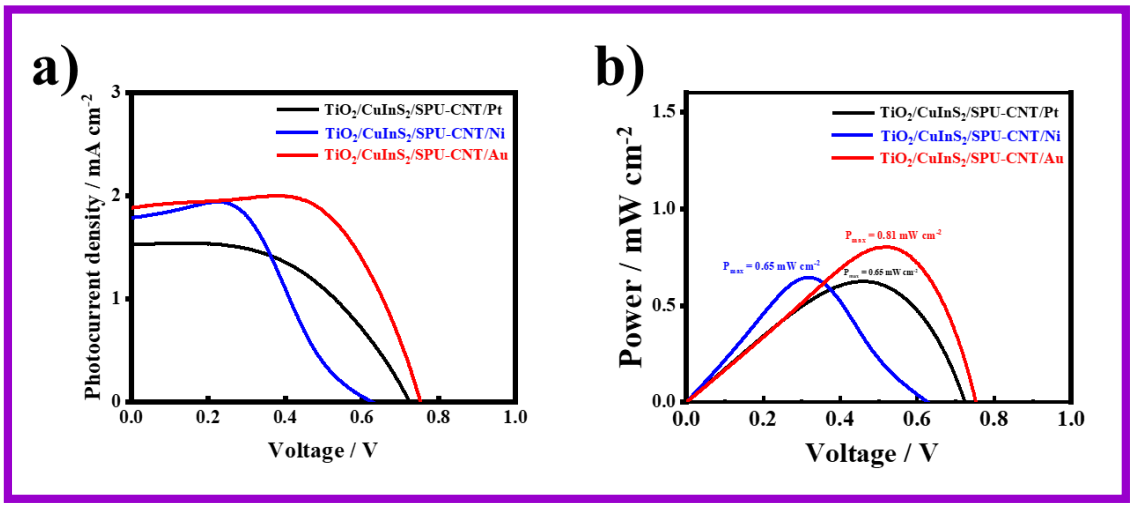

Figure 5.10: (a) *J-V* characteristics measurements to calculate the photocurrent density and open-circuit voltage under 1 Sun illumination (100 mW cm^{-2}); and power-voltage curve to calculate the power conversion efficiency (PCE) of the indicated QDSSCs.

Table 5.3 represents the photocurrent density (J_{max}), open circuit voltage (V_{oc}), fill factor (FF) and power conversion efficiency (PCE) for fabricated cells with various counter electrodes. Nickel work function energy levels value and the performance of the nickel based device is a function of

annealing temperature.[188,189] Then, fabrication of the QDSSCs with same $TiO_2/CuInS_2$ photoanode, developed polymer gel electrolytes (SPU-CNT) and nickel as a counter electrode was made which exhibit improved power conversion efficiency from (η) = 0.62 to 0.65 % and photocurrent density increases from 1.55 to 1.85 mA cm^{-2}, while there is slight reduction in the open circuit voltage (0.64 V), and the fill factor (FF = 0.54). So, need of another counter electrode whose work function energy levels value is closer to the HOMO energy levels of the prepared polymer electrolytes (SPU-CNT). Sachtler et. al., reported the thin film of the gold sintering at 200 ^0C, works function value of 5.38 eV.[190] Hence, we prepared the QDSSCs with Au (gold) counter electrode and $TiO_2/CuInS_2$ photoanode by using the developed SPU-CNT gel electrolytes and obtained the 0.81 % power conversion efficiency with high fill factor (0.57), open circuit voltage (0.74 V) and higher value of the photocurrent density value 1.92 mA cm^{-2}, and which is ~30 % more than the platinum electrode device with similar polymer gel electrolytes and photoanode in QDSSCs. The fabricated device has high fill factor value (0.57) and high open circuit voltage (0.74 V) and produced the higher photocurrent density of 1.91 mA cm^{-2}. The high performance of the fabricated devices with Au counter electrode is due to closer proximity of energy levels between HOMO levels of the prepared polymer gel electrolytes and VB of $CuInS_2$ QDs (0.02 eV) as well as energy level of the Au counter electrode and HOMO levels of the prepared polymer gel electrolytes (0.01). In both cases, the hole transportation rate is greater from VB of QDs to the HOMO levels of the prepared polymer gel electrolytes and further hole transportation rate is also very fast form the HOMO levels of SPU-CNT polymer gel electrolytes to the Au counter electrode. In brief, the developed SPU-CNT polymer gel electrolyte behaves as an efficient hole transport materials in the fabricated QDSSCs by using various counter electrodes (Pt, Ni and Au).

Table 5.3: Photocurrent density, open circuit voltage, fill factor, and power conversion efficiency of various cells using the SPU-CNT polymer gel electrolytes, $TiO_2/CuInS_2$ photoanode and prepared various counter electrode.

S.N.	Photoanode	Counter electrode	Photocurrent density ($mA\ cm^{-2}$)	Open circuit voltage (V)	Fill factor	Efficiency (%)
1.	$TiO_2/CuInS_2$	Pt	1.55	0.71	0.56	0.62
2.	$TiO_2/CuInS_2$	Ni	1.85	0.64	0.54	0.65
3.	$TiO_2/CuInS_2$	Au	1.92	0.74	0.57	0.81

5.7 Conclusion

The successful functionalization was carried out of the MWCNTs and further tagged with the main chain of the polyurethane polymer. The sulfonation of the MWCNTs tagged polyurethane polymer was takes places by using the propane sultone as a sulfonating agent. The all functionalization was confirmed through ^{1}HNMR, FTIR and UV-vis spectroscopic measurements and Raman spectroscopic technique was also used the confirmed the functionalization of polymer. The thermal stability measured through the using the thermogravimetric analysis measurements and the melting temperature was estimated through differential scanning calorimetry. The carbon nanotubes increase the electrical conductivity of the thermoplastic polyurethane due to presence of π-framework in tubes which provide the medium for the transportation of the charge carries. The ionic polar pendent moiety was further enhanced the conductivity of the CNTs-tagged PU (SPU-CNT) and electrical conductivity of the prepared polymer is 1.367×10^{-4} S cm^{-1}, hence, the developed polymer is suitable for the preparation of gel electrolytes (hole transport materials) for

QDSSCs. The CV measurements was used to calculate the HOMO and LUMO energy levels of the functionalized polymer. The active materials $CuInS_2$ QDs was synthesized by using the DDT as a capping agent and their particles sized was measured through TEM bright field images. The optical band gap of the synthesized QDs and relatives light harvesting efficiency of photoanode was calculated by using the light absorption measurements. Three type of the counter electrode was used in QDSSCs such as platinum, nickel and gold. The fabricated devices by using the SPU-CNT polymer gel electrolytes with gold as a counter electrode shows the better performance and the power conversion efficiency 0.81 % was obtained. The devices show the high performances is due to suitable matches of the HOMO energy levels of the developed polymer electrolytes with the energy levels of the gold counter electrode. The limitation of the experimental work is to fabricate and measure the device performance in inert atmosphere.